A00-33844

AIAA 2000–2461
The Effect of a Changing Aspect Ratio Through a Wind Tunnel Contraction

John Callan and Ivan Marusic

University of Minnesota
Minneapolis, MN

Fluids 2000
19–22 June 2000 / Denver, CO

Paper # 2000-2461

THE EFFECT OF A CHANGING ASPECT RATIO THROUGH A WIND TUNNEL CONTRACTION

John Callan* and Ivan Marusic**
Department of Aerospace Engineering & Mechanics,
University of Minnesota, Minneapolis, MN 55455

Abstract

In this study, an attempt is made to determine the effect of changing the Aspect Ratio through the length of a wind tunnel contraction on the flow quality at exit. For this purpose, a parametric study of this specific feature is presented, a design rule of useful cross section area versus AR is produced (i.e. flow uniformity issues), an examination of the flow in the corners and on the walls at exit is presented, and an explanation of the observed varying boundary layer thicknesses between different AR's will be attempted. A specially written CFD code which solves the potential flow equation in the contractions will be used to aid in this discussion.

Nomenclature

A = area of cross section
AR = aspect ratio of cross section
b = half-width
C_f = skin friction coefficient
C_p = pressure coefficient $= 1-\left(\frac{u}{U_e}\right)^2$
D = 'effective' diameter
h = half-height
H = shape factor $=\frac{\delta^*}{\theta}$
H_e = exit height of contraction
Γ = cross sectional area diagonal length
L_c = contraction length without extensions
L_e = extended contraction length
U_e = velocity far downstream of exit
u,v,w = streamwise, normal, spanwise velocity
W_e = exit width of contraction
x,y,z = streamwise, normal, spanwise coordinates
x_m = curve matchpoint
α = floor coordinate
β = side wall coordinate
ξ, η, ζ = 'computational' coordinates
δ^* = displacement boundary layer thickness
δ = 99% boundary layer thickness
ϑ = convergence parameter
λ = cross-stream diagonal coordinate
ϕ = velocity potential
θ = momentum thickness

1. Introduction

The contraction section of a wind tunnel is that component where the flow is accelerated from the settling chamber to working section velocities. Its purpose is to provide a low turbulence, uniform stream into the working section. The design of contractions has been an area of much research in the past. Most theoretical and computational studies have focused on the solution of inviscid irrotational flow equations to establish design rules and guidelines for the optimum design of a contraction. Most early work has been concerned with the analytical solution to

---

* Research Assistant, Member AIAA
** Assistant Professor, Member AIAA

these equations (Tsien 1943, Thwaites 1946, Cohen & Ritchie 1962, Jordinson 1961). The mathematics involved makes implementation of the solutions difficult and in addition, the analytical solutions are only valid for infinitely long contractions with exponentially decaying ends. Later work focused on finding numerical solutions to the inviscid flow equations in a contraction. Of these, Morel (1975) is perhaps the best known. Morel studied an axisymmetric contraction of finite length and produced a series of design charts, giving the designer a tool for optimizing contraction length, contraction ratio and curve matchpoint based on the criteria of the possibility of separation in the contraction, along with the exit flow non-uniformity. From this it was concluded that a curve consisting of two matched cubic arcs, whose matchpoint is a varying parameter, to be the best shape for the contraction.

Later work by Su (1991) considered the design of three-dimensional, or rectangular end contractions using a numerical solution to the three-dimensional Laplace equation. Based on the Morel criteria, Su shows that three-dimensional contractions exhibit poorer qualities, in terms of the possibility of flow separation and exit flow nonuniformity, than axisymmetric contractions with similar geometric properties (contraction ratio etc). The explanation given is that the presence of corners in the three-dimensional case produces greater velocity extrema than in the axisymmetric case. A feature which is present in three-dimensional contractions and not in axisymmetric ones is the effect of "crossflow" in the contraction. Su showed that the crossflow is induced due to the transverse pressure gradient existing in the contraction. This pressure gradient exists because of greater local velocity extrema at the corners relative to the centerline velocities on the walls on the planes of symmetry. A "crossflow parameter" was considered which showed the relative strengths of the crossflow effect for different contraction designs. No conjecture was attempted however, on the effect of this crossflow on the flow quality at exit, specifically on its effect on boundary layer development. Su performed a parametric study by varying the important design parameters and studying their effect on the criteria set out by Morel.

These previous studies, and others (Mikhail 1978 and Fang 1991) have focused on the numerical solution to the flow *in* the contraction for use as a tool for predicting the flow quality at exit. One study, Tulapurkara & Bhalla (1988) performed an experimental analysis of the flow in a contraction, in an attempt to verify Morel's predictions. No studies however have focused on the actual flow in the working section at the exit of a contraction and the effect of changing the geometric parameters of the contraction on it.

No previous studies have looked at the role that changing the Aspect Ratio (AR) through the length of the tunnel has on the corner boundary layers. Designers have generally used "rules of thumb" to guide them. One of these is the so-called "Pyramid Rule" (A.E. Perry, *private communication*) which states that AR should be held constant throughout the contraction in order to minimize the growth of the corner boundary layer vortices into the working section of the wind tunnel. This "rule" conflicts with the conclusion of Su (1991) that changing AR can be advantageous when separation criteria are considered. However, since Su's study is based on solutions to potential flow, no rational comparison can be made. Maintaining a constant AR through the length of the contraction can often be impractical because of space constraints and also becomes a trade-off between varying other important parameters such as a higher contraction ratio, for example.

In this paper, we wish to address the issue of changing the AR through a contraction by:

1) Keeping shape fixed
2) Keeping Contraction Ratio (CR) fixed
3) Keeping length fixed
4) Keeping inlet AR fixed at 1 and varying exit AR

2. Experimental Procedure

Four contractions were constructed and were fitted to an existing wind tunnel facility, each with fixed values for the various geometric parameters, with the exception of exit AR. The values of the fixed parameters used in this paper are given in table 1.

Inlet Area A_i *(mm²)*	*Contraction Ratio (CR)* A/A_e	*Contraction Length / Inlet Diameter* L_c / D_i
600 x 600	8.72	1.0
Contraction length L_c *(mm)*	*Matchpoint* x_m/L_c	*Exit Reynolds no.* Re_e
686	0.6	4.8×10^5

Table 1

The length of the contraction is denoted as L_c ; D_i is the effective inlet diameter and is given by:

$$D_i = \sqrt{\frac{4A_i}{\pi}} \qquad (1)$$

x_m is distance from the beginning of the contraction to the matchpoint of the cubic curves. The Aspect Ratio is defined as the width/height.

The Reynolds number (Re_e) is based on the exit velocity and exit effective diameter. The exit AR variation is given in table 2.

AR	**Exit Dimensions** (mm)
1	203 x 203
2.25	305 x 135
3	356 x 116
4	406 x 102

Table 2. Exit AR variation

The contours of the curves are defined in the same manner as those used by Su (1991). Full details of the design and construction of the contractions are given in Callan (2000).

In addition, a short working section was attached to the exit of the contraction.

Streamwise velocity and turbulence intensity measurements were made with a single component hot-wire, one effective exit diameter downstream of the contraction exit, as shown in figure 1. Data was gathered across the plane with the wires oriented both parallel to the floor and parallel to the side wall. In addition, wall boundary layer profiles on the centerlines of the floor and side wall respectively were obtained using the hot-wires. Corner boundary layer profiles were obtained with the wire oriented perpendicular to the 45° axis of the corner, similar to those performed by Zamir and Young (1970).

For all measurements, 5μm single Wollaston wires, with an etched length of nominally 1mm were used with a DANTEC normal wire probe support. A TSI IFA-100 anemometer was operated with an overheat ratio of 1.8 and the signals were conditioned and digitized with 16-bit resolution. The hot-wire signals were sampled at a rate of 500Hz and 15000 samples were taken per point. Data was stored and processed on a PC using Matlab. The hot-wires were calibrated statically using a 3rd order polynomial curve fit.

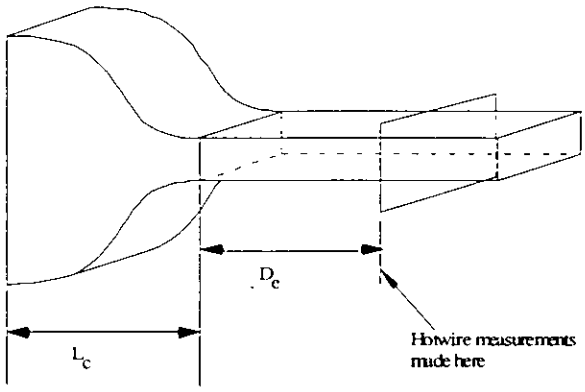

Figure 1: Location of experimental measurements

3. Computation

In order to quantify the pressure gradients and other parameters in the contractions, a numerical solution to the three-dimensional Laplace equation (equation 2) was undertaken for the contractions used here. Only the basic method of computation is presented here since it is similar to that used by Su (1991); a more complete description is given in Callan (2000).

The solution to Laplace's equation, given as:

$$\frac{\partial^2\phi}{\partial x^2}+\frac{\partial^2\phi}{\partial y^2}+\frac{\partial^2\phi}{\partial z^2}=0 \qquad (2)$$

represents an irrotational, inviscid "potential" flow which in a contraction is assumed a useful and accurate tool for analyzing the flow in a real contraction due to the fact that the boundary layers are thin on the walls of the contraction, and assuming that separation does not take place anywhere in the contraction.

The solution employed for this study is a simple pointwise finite differencing scheme with no relaxation. A body-fitted coordinate system is used to transform the physical domain to the computational domain (equation 3).

$$x = L_e\xi; \qquad y = h(x)\eta; \qquad z = b(x)\zeta \qquad (3)$$

where $h(x)$ and $b(x)$ define the floor and side wall curves respectively. The physical domain is mapped

into a unit cube in computational space, with ξ,η and ζ varying from 0 to 1 respectively, as shown in figure 2. The metrics of transformation are obtained by finite differencing of the differential equations. Because of the nature of equation 2 (it being elliptical), extended straight sections are added to the beginning and end of the contraction for the computation (not shown in figure). L_r represents the length of the entire contraction with extended sections.

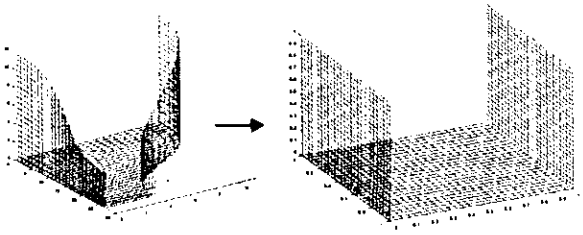

Figure 2: Discretization of Boundaries

The boundary conditions are such that the surfaces are assumed to be streamlines of the flow and as such there is no flow normal to them. Because of symmetry, only one quadrant of the contraction was examined for each contraction. Thus, a further boundary condition is that there is no flow normal to the planes of symmetry along their centerlines. The boundary conditions at inlet and exit are that all flow is in the streamwise direction, therefore ϕ can be fixed across the plane at these locations, and can be set equal to 0 and 1 respectively without loss of generality.

A grid of 27×27×27 points is used and no numerical instability is found. The residual error ($\phi^{n}_{i,j,k} - \phi^{n-1}_{i,j,k}$) is of the order of 10^{-6}.

4. Results and Discussion

4.1 Wall Boundary Layers

A principle feature of the effect of AR change through a contraction is its effect on the development of the boundary layers on the walls and in the corners of the contraction. Bradshaw (1973) shows that boundary layer development is controlled not only by streamwise pressure gradients, but also by the effect of the extra straining caused by a diverging or converging flow. Following Saddoughi & Joubert (1991), this extra straining can be denoted by a "convergence parameter" in a nominally two-dimensional boundary layer as:

$$\vartheta = -\frac{1}{U}\frac{\partial w}{\partial z} \quad or \quad \vartheta = -\frac{1}{U}\frac{\partial v}{\partial y} \tag{4}$$

depending on orientation, where ϑ is the convergence parameter, U is the streamwise velocity, w and v the spanwise and normal velocities respectively, and z and y the spanwise and normal coordinates respectively. A diagram showing streamwise convergence is given in figure 3.

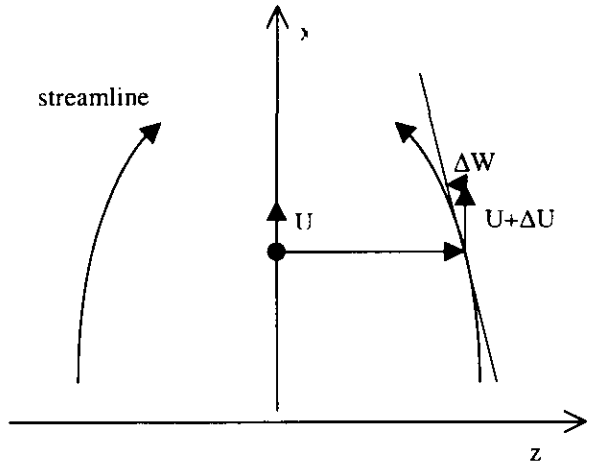

Figure 3: Streamline convergence

This convergence parameter can be included in the momentum-integral equation for boundary layers in the centerline plane as:

$$\frac{d\theta}{dx} = \frac{C_f}{2} - (H+2)\frac{\theta}{U}\frac{dU}{dx} + \vartheta\theta \tag{5}$$

Where θ is the boundary layer momentum thickness, C_f is the skin friction coefficient, H is the boundary layer shape factor and U is the velocity in the freestream outside the boundary layer.

For diverging flows, the sign of the convergence term is reversed.

The effect of the streamline convergence present in a contraction will be examined in this section of the paper and will be used to aid in quantifying the effects of changing AR on the boundary layers, and hence the overall exit flow quality.

Figure 4 shows the streamwise pressure history obtained from numerical analysis along the floor and side wall at the respective planes of symmetry (centerlines), for AR 1 and AR 4. For any contraction of this type, there exists two regions of adverse pressure gradient on the walls: one near the inlet and another near the exit. It can be seen from figure 4 that there is a difference in C_p in the inlet region on the side wall and floor for the AR 4 contraction. However, their respective pressure histories become very closely matched in the exit section. On the other hand, the pressure history of the AR 1 case (which is the same on all walls due to symmetry) is markedly different than either of the AR 4 walls. Figure 5 shows the change of ϑ along the floor and side walls of both AR 1 and AR4 contractions, on their centerlines. The value of ϑ for AR 1, which due to symmetry will have the same floor and wall ϑ, falls between the values of AR 4 floor and AR 4 side wall. The AR 4 case shows that the maximum value of ϑ for the side wall is over 3 times larger than for the floor.

From equation (5), assuming an equivalent streamwise pressure history and friction coefficient between two boundary layers, the phenomenon which controls their development through a contraction is ϑ. However, figure 4 shows that the pressure histories between different AR's as well as between the side wall and floor for a given AR>1 are different. This illustrates the fact that the boundary layer developments in a contraction are unique to each particular contraction. Comparisons of exit boundary layer thicknesses between different AR's is therefore not straightforward. Comparisons of boundary layers within a particular contraction is slightly more straightforward however. Figures 4 and 5 show that the dominant effects for a particular AR are the variation of ϑ and C_p on the side wall and on the floor respectively. Figure 5 shows that, for a given contraction, the boundary layer on the side wall will be thicker than that on the floor, for AR >1. This is due not only to the different pressure histories between the side wall and floor, but also to the difference in streamline convergence between the two. Figure 6 shows the exit boundary layer thicknesses, δ, along the centerlines of the side wall and floor respectively, one exit diameter downstream of exit. Here δ is taken to be δ_{99}, the point at which the mean velocity in the boundary layer is 99% of the freestream mean velocity. They show a general trend of bottom boundary layer thinning with increasing AR and no clear trend for the side boundary layers. These results highlight the fact that a comparative study of wall and floor boundary layer thicknesses between different AR's is not a relative comparison, because of the different pressure histories and convergence parameter values. However, a comparison of side boundary layer thickness vs. bottom boundary layer thickness for a given AR shows that generally, for AR >1, $\delta_{side} > \delta_{floor}$, as is expected.

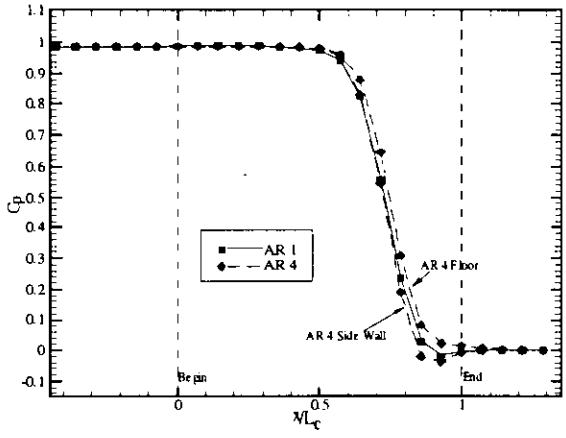

Figure 4: C_p on side walls & floor

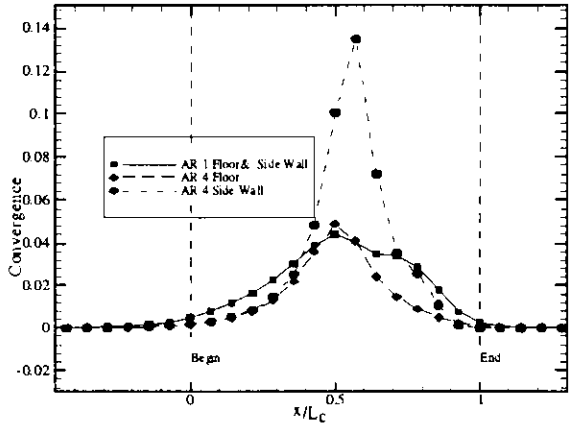

Figure 5: ϑ on side walls & floor

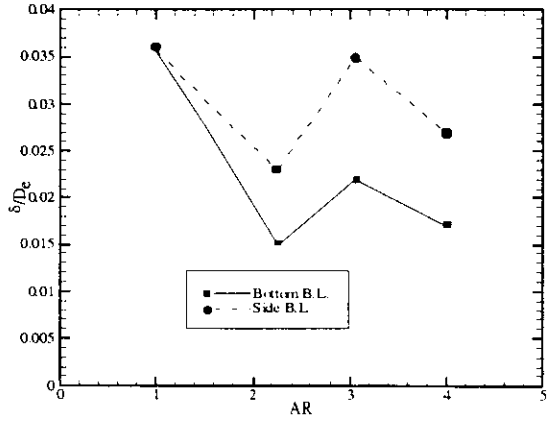

Figure 6: Bottom & Side boundary layer thicknesses

4.2 Corner Boundary Layers

A second feature of interest when examining the effect of AR change in a contraction is the change in corner boundary layer flow. The variation of C_p through a contraction on the corner, as calculated using the potential flow solution, is shown in figure 7 for AR 1 and 4 respectively. It can be seen that the points of maximum and minimum velocity in a three dimensional contraction occur in the corners. The respective inlet histories of AR 1 and AR 4 are similar, with AR 1 showing a more pronounced inlet adverse pressure gradient, but it is at the exit region where the differences are most noticable. AR 1 has a significant region of adverse pressure gradient at exit, whereas for AR 4 the adverse gradient is less pronounced. One would expect the boundary layer at the corner to be larger for AR 1 than for AR 4 because of this effect. This is shown to be true in figures 8 and 9 respectively. Figure 8 shows the corner boundary layer thicknesses (ξ^{45}) measured along a 45° line from the corner, one exit diameter downstream of exit. It can be seen that the boundary layers get thinner with increasing AR. Figure 9 shows their respective mean velocity profiles.

Figures 10 to 13 show contour plots of measured mean velocity and turbulence intensity ($Tu = \frac{\sqrt{\overline{(u-\bar{u})^2}}}{U}$) in the lower left hand corner of the exit plane, one exit diameter downstream of exit. For all contour plots, data is taken with the hot-wire normal to the floor for the sections to the right of the diagonal, and normal to the side wall for the sections to the left of the diagonal as one views it on the page. Figures 10 and 11 show mean velocity contour plots for AR 1 and AR 4 respectively. Figures 12 and 13 show turbulence intensity contour plots for AR 1 and AR 4 respectively. The corner boundary layers are seen to have undergone transition to turbulence.

Previous studies have been conducted on turbulent corner boundary layer flows. In their experimental study of a turbulent corner boundary layer, Nakamura et al (1987) show the presence of two counter-rotating vortices in a turbulent corner boundary layer aligned either side of the 45° line of an arbitrary "infinite" corner. Due to the small physical size of the boundary layers in the corners, only streamwise

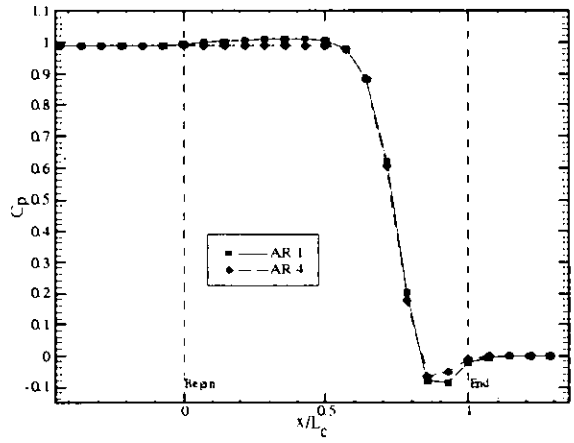

Figure 7: Cp on corners

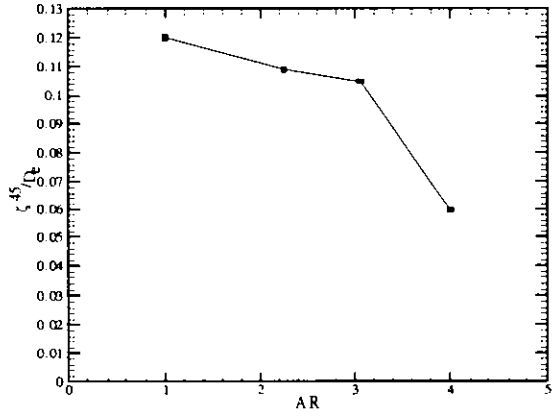

Figure 8: 45° corner boundary layer thicknesses

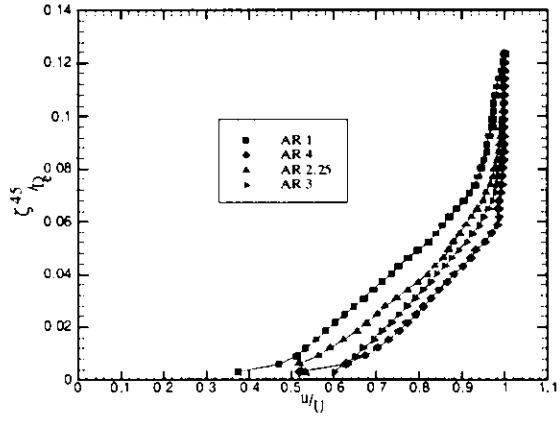

Figure 9: 45° corner boundary layer mean velocity profiles

velocity measurements were made. In the absence of spanwise and normal component velocity measurements, it is difficult to quantify these vortices. However, an examination of the turbulence intensity contour plots (figures 12 and 13) shows a region of high turbulence intensity close to the floor and to the right of the diagonal line. It is seen that it is more prominent in the AR 4 case. One can assume the presence, however small, of these counter-rotating vortices in the corner. The effect of the extra strain rate on the nature and orientation of the vortices imposed by the streamline convergence

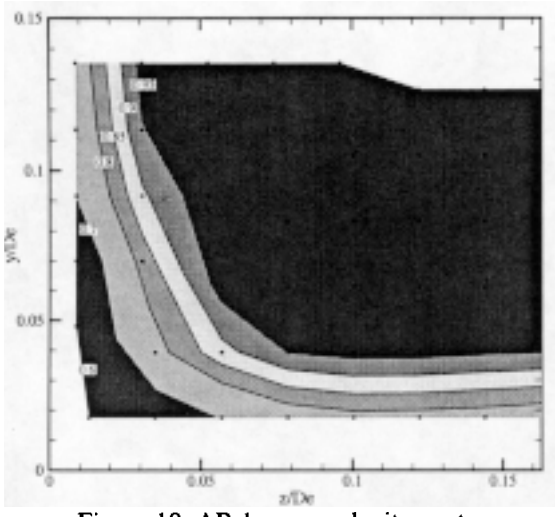

Figure 10: AR 1 mean velocity contours

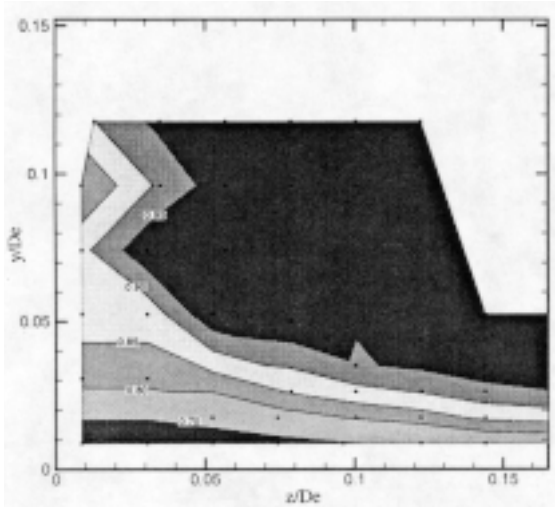

Figure 11: AR 4 mean velocity contours

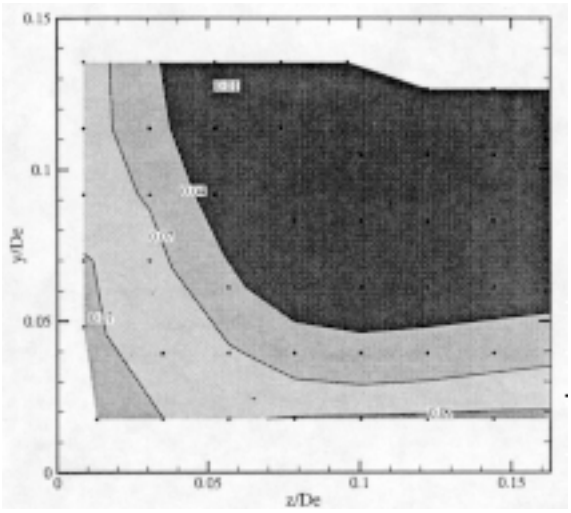

Figure 12: AR 1 turbulence intensity contours

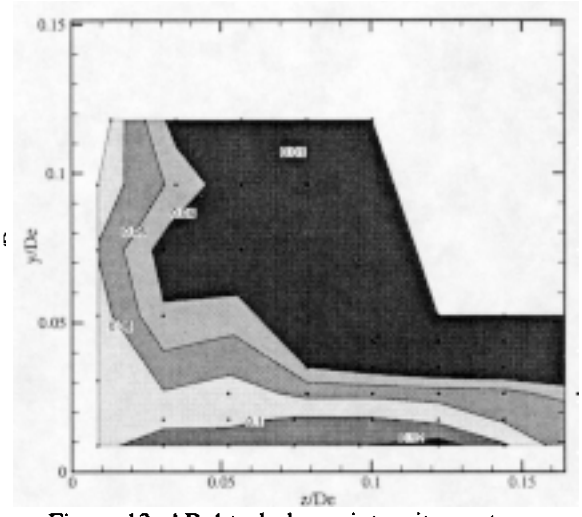

Figure 13: AR 4 turbulence intensity contours

difference (for AR >1) upstream is unclear. However, figure 14 shows the mean velocity profile along the diagonal of AR 1 to 4 inclusive, one exit diameter downstream of exit. Data is interpolated from the mean velocity contour plots. Furthermore, it shows a collapse of the data along this diagonal. It shows that at about 0.08Γ along this diagonal (Γ being the diagonal length for a given AR), the corner layer ends. This surprising result would suggest that perhaps the principle orientation of the vortices in the corners of a confined duct are not about the 45^0 line but are in fact about the diagonal line. The data given here can only suggest that, and further studies would need to be performed.

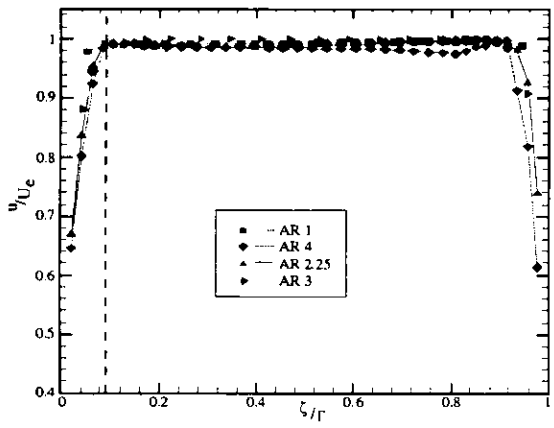

Figure 14: Diagonal mean velocity profiles

Section 4.3 Useful Working Area

Of more practical interest, the results in figure 14 can be used as the basis of an approximate design rule for contractions with varying AR. Figure 15 shows a schematic of the "Useful Area" of a working section downstream of a contraction exit. Here the useful area is defined as that region where the flow has low freestream turbulence (i.e. outside the boundary layers) and has high uniformity across the plane. Hence, it is the area where useful and practical measurements can be made in the working section of a wind tunnel.

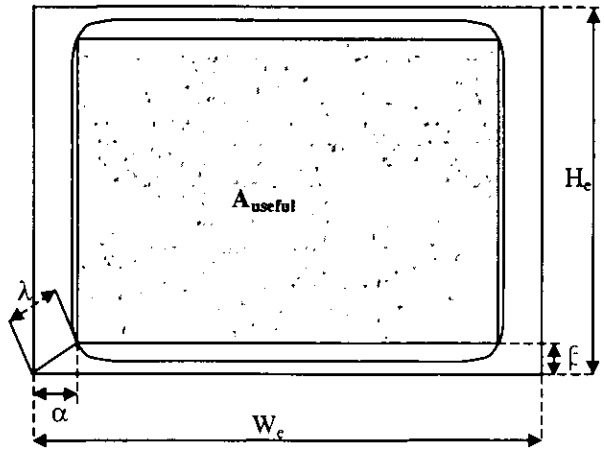

Figure 15: "Useful Area" of exit plane

From the following analysis, an approximate design rule can be established.

From figure 14, along the diagonal the boundary layer ends at

$$C = \frac{\lambda}{\Gamma}\left(= \frac{\alpha}{W_e} = \frac{\beta}{H_e}\right) \cong 0.084$$

where λ, α, and β are shown in figure 15.

Thus,

$$\beta = CH_e; \qquad \alpha = CW_e \tag{6}$$

The total cross sectional area is

$$A_o = W_e H_e \tag{7}$$

and the useful area is

$$A_{useful} = (W_e - 2\alpha)(H_e - 2\beta) \tag{8}$$

From equation 6 the useful area becomes:

$$A_{useful} = A_0(1-2C)^2 = 0.69A_o \tag{9}$$

Equation 9 gives the estimated useful cross sectional working area based on the total cross sectional area only. This result shows that there is no dependance on the useful area with Aspect Ratio. However, this analysis can be used to determine the "useful width" and "useful height" of the working section based on exit AR by simply using the results from figure 14.

5. Conclusions

An experimental and computational analysis of the effect of changing the Aspect Ratio through a three-dimensional wind tunnel contraction has been performed. This has been done by measuring the boundary layers at the exit of the contractions on the side walls and floors. Their development is related to the pressure history on the wall, as well as to the effect of streamline convergence. Noteworthy results include:

- Comparisons between contractions with different AR's show that pressure histories are the dominant effect when performing comparisons of boundary layer thicknesses on the same wall of the contraction.
- For a given AR, comparitive results between side wall and floor boundary layers show that for AR >1 the side wall boundary layer will be thicker than the exit boundary layer.
- The 45^0 corner boundary layer thicknesses decrease with increasing AR. Computational

pressure histories indicate the strenghtening of adverse pressure gradients close to exit as AR approaches 1.

- An examination of the mean velocity profile along the diagonal of the exit plane reveals a collapse of data. From this, an approximate design rule for the estimation of "useful area" in the working section, and an approximation of the extent of the boundary layer region for both side and floor wall has been proposed.

References

Bradshaw, P., "Effects of Streamline Curvature on Turbulent Flow", *AGARD-AG*-169, NATO, 1973

Callan, J. "The Effect of a Changing Aspect Ratio through a Wind Tunnel Contraction", *Masters Thesis, University of Minnesota,* 2000.

Cohen, M.J., and Ritchie, N.J.B., "Low-Speed Three Dimensional Contraction Design", *Journal of Royal Aeronautical Society*, Vol. 66, 1962, pp.231-236

Fang, F., "A Design Method for Contractions with Square End Sections", *Journal of Fluids Engineering, ASME Transactions,* Vol. 119, June 1997, pp. 454-458.

Jordinson, R., "Design of Wind-Tunnel Contractions", *Aircraft Engineering,* Vol. 33, 1961, pp.294-297

Mikhail, M.N., "Optimum Design of Wind Tunnel Contractions", *AIAA Journal,* Vol. 17, No. 5, 1979, pp.471-477.

Morel, T., "Comprehensive Design of Axisymmetric Wind Tunnel Contractions", *Journal of Fluids Engineering, ASME Transactions,* Series I, Vol. 97, June 1975, pp.225-233.

Nakamura, I., Miyata, M., Kushida, T., Kagiya, Y., "An Experimental Study of the Intermittant Region of a Corner Turbulent Boundary Layer", *JSME International Journal,* Vol. 30, No. 259, 1987 pp.72-79.

Saddoughi, S.G., & Joubert, P.N., "Lateral Straining of Turbulent Boundary Layers, Part 1. Streamline Divergence", *Journal of Fluid Mechanics,* Vol. 229, 1991, pp.173-204.

Su , Y., "Flow Analysis and Design of Three-Dimensional Wind Tunnel Contractions", *AIAA Journal,* Vol. 29, No. 11, April 1991, pp. 1912-1920.

Thwaites, B., "On the Design of Contractions for Wind Tunnels", *ARC,* R&M 2278, 1946

Tulapurkara, E.G. & Bhalla, V.V.K., "Experimental Investigation of Morel's Method for Wind Tunnel Contractions", *Journal of Fluids Engineering, ASME Transactions,* Vol. 110, March 1998, pp. 45-47

Tsien, H.S., "On the Design of the Contraction Cone for a Wind Tunnel", *Journal of Aeronautical Sciences*, Vol. 10, 1943, pp.68-70

Zamir, M., & Young, A.D., "Experimental Investigation of the Boundary Layer in a Streamwise Corner, *Aeronautical Quarterly,* November 1970, pp.313-339